JOURNAL OF GEOPHYSICAL RESEARCH, VOL. 101, NO. A7, PAGES 15,605–15,613, JULY 1, 1996

On the formation of wave packets in planetary foreshocks

L. Muschietti, I. Roth, and R. E. Ergun

Space Sciences Laboratory, University of California, Berkeley

Abstract. Kinetic localization of beam-driven Langmuir waves is studied for parameters relevant to the electron foreshock environment. Particle-in-cell simulations of the interaction occurring between energetic electrons and Langmuir waves are performed. It is shown that the nonlinearities in the resonant electrons lead to the formation of packets growing out of the noise. The characteristic spatial scale depends upon the beam velocity and has a weak dependence on the wave amplitude. The mechanism takes place within shorter timescales and for smaller amplitudes than the classic nonlinearities due to bulk electrons and ions. As an example, we apply the results to observations made in the Earth and Jovian foreshocks.

1. Introduction

Bursts of Langmuir waves have been repeatedly measured by satellites in the solar wind upstream of planetary bow shocks. The waves are driven by fluxes of energetic electrons that flow back from the shock into the solar wind [*Filbert and Kellogg*, 1979; *Fitzenreiter et al.*, 1984]. Recent observations from the WIND spacecraft [*Fitzenreiter et al.*, 1995] confirm the formation of bump-on-tail reduced velocity distributions due to the combined effects of electron mirroring at the shock and time of flight. The Langmuir emissions are bursty and the wave envelopes are highly structured, displaying strong modulations [*Hospodarsky et al.*, 1991; *Thiessen and Kellogg*, 1993]. Our purpose is to explore the role kinetic localization of beam-driven Langmuir waves [*Muschietti et al.*, 1995] (hereinafter referred to as MRE) might play in the electron foreshock environment. In MRE we showed, using particle-in-cell simulations (PIC) with open boundaries and realistic distribution functions, that the wave energy deposited by a tenuous beam of electrons is not uniform yet tends to localize. The phenomenon is due to nonlinearities in the resonant electrons, hence takes place for smaller amplitudes and on much shorter timescales than the classic Zakharov-type focusing associated with the ponderomotive force.

The Langmuir wave emissions observed near the edge of the Earth's foreshock are narrow-banded about the electron plasma frequency f_{pe} (20 to 50 kHz), and have typical intensities of 0.1—1 mV/m [*Etcheto and Faucheux*, 1984; *Lacombe et al.*, 1985]. Peak values in the 10-mV/m range have also been reported [*Filbert and Kellogg*, 1979]. The wave field is electrostatic and mainly directed along the interplanetary magnetic field, although the burstiness of the waves renders this determination difficult. A statistical study of burst durations indicates a characteristic ~30-ms time [*Lacombe et al.*, 1985]. This feature suggests that the electrostatic power is distributed in localized packets that pass by the satellite; considering convection by a 300-km/s solar wind, a 30-ms burst corresponds to a ~10-km packet size, or $\sim 10^3$ debye lengths (λ_d). Similar Langmuir waves are observed near the edge of the Jovian foreshock [*Thiessen and Kellogg*, 1993]. They have typical intensities of 0.1—1 mV/m and display strong envelope modulations, an example being shown in Figure 1. In fact, the foreshock regions of essentially all the planets seem to exhibit similar Langmuir wave emissions [see e.g. *Scarf et al.*, 1983; *Skalsky et al.*, 1993; *Hospodarsky et al.*, 1994].

Since the waves are due to energetic electrons streaming back from the bow shock, understanding the details of the wave-electron interaction is of importance. The interaction plays a basic role in the growth of the waves and, presumably, in their nonlinear evolution as well. Consider an electron representative of the population believed to provide the free energy for the electrostatic field [*Fitzenreiter et al.*, 1984]; its velocity along B is of order $v_\parallel \sim 8 \times 10^6$ m/s, that is, $v_\parallel/v_e \sim 6$ where v_e is the electron thermal velocity, while the associated resonant wavelength is $\lambda = v_\parallel/f_{pe} \sim 300$ m. Consider now a packet of 300-m wavelength waves localized over 10 km. The electron crosses the wave packet in $\tau_t \approx 1$ ms. The transit time τ_t is comparable to the bounce time $\tau_b = (m\lambda/eE2\pi)^{1/2}$ of a resonant electron in a $E = 0.3$ mV/m sinusoidal wave, a typical intensity in the foreshock. This observation suggests some link between the size of the packet and the nonlinear motion of the resonant electrons responsible for driving up the wave field. Of course, considering the variations and uncertainties in the data about the wavelength, the size of the packet, and the value of the electric field, τ_t and τ_b are equal only in an order of magnitude sense. However, and even though no dedicated search through the data

Paper number 96JA00926.
0148-0227/96/96JA-00926$09.00

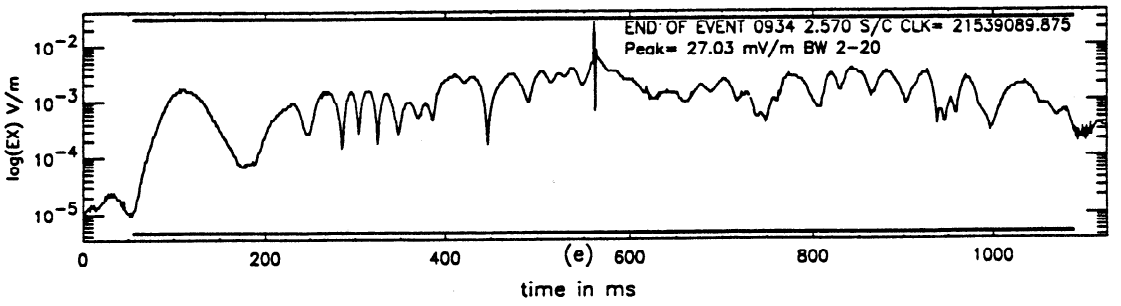

Figure 1. Example of a high-resolution Langmuir wave envelope observed in the Jovian foreshock. Note the modulations and ignore the spike in the middle which is not under consideration here [from *Thiessen and Kellogg*, 1993].

set has so far been done to prove it, the simulations we present below show that this equality may indeed not be accidental.

Localized wave packets can be produced by strong turbulence processes. During the coupled evolution of an ensemble of Langmuir and ion acoustic waves, the high-frequency wave fields refract into regions of low density, from which their ponderomotive force expels particles. When nonlinear self-focusing and the ponderomotive force overcome the dispersion of the wave packet, the latter contracts and intensifies. A quantity of paramount importance in this description is the ratio of the electrostatic field energy to particle energy, $W = \epsilon_0 E_a^2/(4nT)$ with E_a the amplitude of the electric field envelope. *Robinson and Newman* [1991], on the basis of an extensive series of numerical simulations using the Zakharov equations, found the characteristic formation scale of a wave packet to be $l_i \approx 6\,\langle W\rangle^{-0.5}\lambda_d$ where the angular brackets denote a spatial average. They also determined that the packet would self-focus, or collapse, in a time $\tau_c \approx 36/(\omega_p\,\langle W\rangle)$. Now, a field amplitude of 0.3 mV/m, as considered in the previous paragraph, corresponds to $W \approx 10^{-8}$ in a plasma with a nominal density and temperature of 10 cm^{-3} and 12 eV, respectively. For such weak electric fields strong turbulence would predict wave packets forming on a characteristic scale $l_i \lesssim 300$ km, which require a long time, $\tau_c \approx 10^4$ s, to self-focus. In the foreshock environment such self-focusing is indeed unlikely to occur because the packets will be disrupted by ambient density irregularities beforehand, τ_c being orders of magnitude larger than an estimated disruption time $\tau_d \approx l_i/C_s \approx 6$ s [*Cairns and Robinson*, 1992a].

In *Muschietti et al.* [1994] we studied the effects field localization has upon wave-electron interaction by integrating analytically the Vlasov equation for a given wave packet. Special emphasis was put on the phase relation of the perturbed distribution function to the wave field. The distribution function develops bunch-ellipses in phase space forming a chain of alternating particle enhancements and depletions about the wave phase velocity v_p. In the linear regime the bunches move at the velocity v_p creating an oscillating density (or current) that is mostly resistive, which amplifies the Langmuir wave. Low-noise PIC simulations were carried out with open boundaries and weak field amplitudes (MRE), which enabled us to observe the bunch-ellipses and test our model. In the nonlinear regime the bunch-ellipses develop into a double chain of enhancements and depressions in phase space moving at sligthly different velocities. As in an interference pattern, the associated oscillating density (or current) becomes spatially modulated, determining where growth is enhanced and where it is suppressed. This causes the wave energy deposited by the beam electrons to clump in localized spots, an effect we called kinetic localization.

The simulations of MRE, which were applied to the auroral environment, had the following restrictions: (1) runs were initiated with a "seed" packet artificially excited from outside in order to create a clean field shape well above the noise; (2) runs were carried out for a hundred of plasma periods only and ion dynamics was deliberately ignored. We now relax these limitations and present more general results, while choosing parameters appropriate to the foreshock (section 2). We have the waves grow out of the noise and we allow for ion dynamics by using discrete ions with the real mass ratio in several of our simulation runs. Finally, very long runs are performed (up to 500 plasma periods) in order to elucidate the saturation mechanism. We show that the nonlinearities in the resonant electrons lead to the formation of packets growing out of the noise. The typical length of an individual packet is given by $\mathcal{L} \sim (\pi/\omega_p)(m\omega_p/eE_a)^{1/2}\,v_p^{3/2}$ where v_p is the phase velocity in resonance with the beam and E_a is the electric field amplitude (section 3.1). The saturation is due to wave transport: the free energy lost by the electrons is carried away by the motion of the packets (section 4.1). There is some, yet little, transfer of spectrum in the backscatter direction for the wave intensities achieved (section 4.2). Finally, our simulation results are compared to some observations made by Ulysses in the Jovian foreshock and appear to describe well the amplitude modulations (section 5).

2. Simulation System

2.1 Model

An essential feature of the foreshock is the formation of spatial gradients in the electron distribution function

due to the constant injection of beam energy from the bowshock [*Klimas and Fitzenreiter*, 1988]. This leads to a continuous regeneration of the bump despite quasilinear relaxation. In their Vlasov simulations of the foreshock Klimas and Fitzenreiter described the effect by a source term proportional to the large-scale gradient. Here, we use our open boundary, one-dimensional PIC code (MRE) and simulate the plasma on a small spatial interval which lies along the local magnetic field and drifts (in the shock rest frame) at the solar wind speed. As compared to the foreshock dimension, which is measured in tens of Earth's radii, the interval is small ($\lesssim$100 km) and drifts inside the foreshock by a few kilometers only during the simulation period ($\omega_p\tau \sim 10^3$, i.e., $\tau \sim 5$ ms). The simulation system resembles the actual physical system in that it incorporates nonperiodic boundary conditions for the particles and allows one to inject fresh distribution functions at the ends of the simulation box. From the left end we inject electrons that include the particles reflected from the shock which make a small bump in the reduced distribution. The electrons injected from the right simulate the free solar wind. Particles leaving the system at either ends are ignored.

The actual shape of the distribution function $F_e(v)$, core, halo, and beam, emulates reduced distributions observed in the Earth's foreshock by ISEE 1 [*Fitzenreiter et al.*, 1984, 1990]. We use two models of distribution functions, model I being displayed in Figure 2 and the parametrization given in Table 1. The associated dispersion relation shows that the instability occurs on the Langmuir branch and is limited to the wavenumber range $0.18 < k\lambda_d < 0.26$.

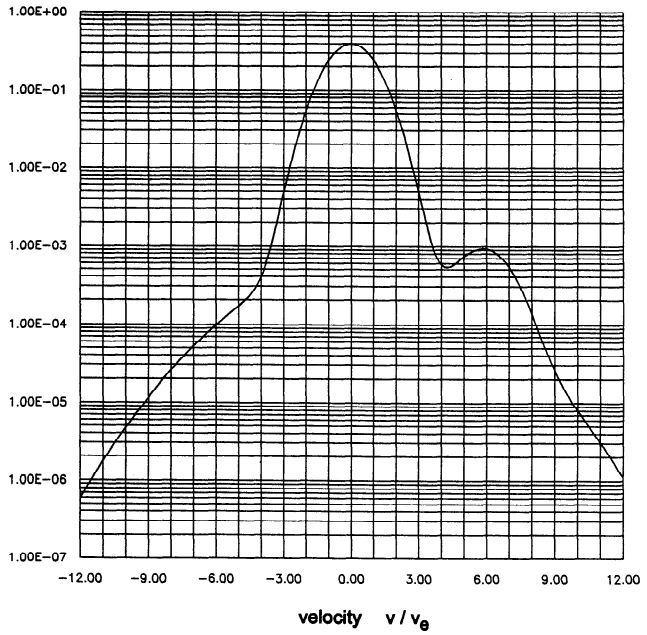

Figure 2. Model I of distribution function used in the simulations. $F_e(v)$ consists of a Maxwellian core, halo, and beam with the parametrization given in Table 1. The velocity is given in units of the thermal core velocity. Read 1.00E+00 as 1.00×10^0.

Table 1. Model of Distribution Function

	Density	Drift	Δv
Core	1.0	0.	1.0
Halo	0.005	0.28	3.3
Beam	0.002	6.0	1.0

The model is made of three populations: core, halo, and beam, each with Maxwellian shape and three parameters (density, drift, and spread). Density and velocities are given in units of the density and thermal spread of the core particles, respectively. The function shown in Figure 2 is for the values above. In model II the halo density is twice larger, which submerges partially the beam, thereby reducing the free energy available.

The purpose of this investigation is to study the local kinetic interaction between Langmuir waves and the electrons that stream along foreshock magnetic field lines. It is assumed that in spite of wave-particle interaction a beam feature in the distribution function has survived the travel from the bow shock to the interval under investigation; the feature may be due to time-of-flight effects [*Filbert and Kellogg*, 1979] and is evidenced by the occasional observation of a bump in the reduced distribution function far away from the shock [*Fitzenreiter et al.*, 1984, 1995]. In the interval, by contrast, Langmuir waves are not prevented from growing and do affect the electrons. These have, however, only a finite time to "feel" the local electrostatic field while they traverse the interval from one end to the other.

2.2 Boundary Conditions, Macroparticles, and Noise Level

In an open system fresh particles continuously enter the simulation box while particles having interacted with the wave field exit. In the duration of one time step the net flux through a boundary is rarely an integer number of simulated macroparticles. Since, on the other hand, the numerical flux is necessarily quantized, a slight charge imbalance is created in the cell adjacent to the boundary. Undesirable fluctuations are generated, which propagate inward. The noise level depends upon the charge e_j carried by one macroparticle. This unwanted noise is especially problematic for fast electrons which penetrate far into the boundary cell during their first time step into the simulation box. The key to achieve low noise is to reduce their charge, hence their discrete effect. Accordingly, we split the distribution function of Figure 2 into different velocity regions and describe the fast electrons with smaller macroparticles than the macroelectrons representing the bulk plasma. The procedure maintains the effective plasma frequency while increasing the numerical flux of particles across the boundary. In addition, it improves the statistics in the velocity region where the interaction with the waves is the strongest and $F_e(v)$ is small. As an example, during each time step we inject through the left boundary 70 particles describing the electron distribution function in the velocity range $7 < v/v_e < 12$. They have a charge (and mass) 225 times smaller than the bulk macroelectrons. Were we to use the latter in that velocity range, we would need to inject 0.31 particle per time step, which due to the quantization of the number

of particles would create a huge fluctuation every three time steps on average.

A constant influx of fresh particles is emitted at both ends of the interval while the particles that leave it are removed from the system. As for the boundary conditions on the potential required to solve Poisson's equation, we use the following. The potential difference between left and right ends is computed by balancing the particle current integrated through the interval with the polarization current, such that the electrostatic character of the field is enforced. In addition, the potential is chosen to be zero at the left (upstream) boundary where we assume no wave activity.

The number of electrons per Debye length, or plasma parameter, varies from 600 to 1000 in our series of runs. The same parameter, it should be pointed out, is at most 100 in standard one-dimensional PIC simulations. The large number of particles together with the division scheme used to handle the injection of fast electrons enables us to keep the noise level at $\epsilon_0 E^2_{\rm rms}/(nT) < 10^{-4}$, a reasonable value by PIC standards. This is, however, still very large as compared to the Langmuir energy density $\mathcal{W} \equiv \epsilon_0 E^2_{\rm rms}/(nT)$ (the definition includes the kinetic energy of wave motion) measured in the solar wind environment. Thus Langmuir waves of 1 mV/m correspond to $\mathcal{W} = 5 \times 10^{-7}$ only, a value well below our noise level. It is clear therefore that PIC simulations with electric field intensities similar to observed levels are not yet today within reach. What is, however, within reach, and impossible in previous simulations, is to work in a regime moderately nonlinear. For example, recent particle simulations of *Dum* [1990a, 1990b] operate with $\mathcal{W} \sim 10^{-3}$—10^{-2}. Current particle simulations in Japan have $\mathcal{W} \sim 10^{-2}$ (Akimoto et al., Rapid Generation of Langmuir Wave Packets during Electron Beam-Plasma Instabilities, submitted to Physics of Plasmas). In ours also the wave energy remains at all times a small fraction of the plasma energy, and we can then meaningfully resort to scaling laws in comparing simulation results to measurements.

3. Emergence of Wave Packets Out of the Noise

Figure 3 shows four successive snapshots of the electric field as a function of position. As time elapses, two packets with a wavelength $\lambda \approx 30\ \lambda_d$ appear near the middle of the simulation box. The waves have a phase velocity $v_p \approx 30/(2\pi) = 4.8\ v_e$, are in resonance with the positive slope of $F_e(v)$ (see Figure 2), and are, of course, growing. Interestingly, they do not grow as one single, coherent packet extending over a distance $500\ \lambda_d$ or more, but as two packets separated by a short region of phase uncertainty and weaker amplitude. A blowup (not shown) reveals that the phase of the downstream packet (on the right) lags by $\pi/2$ behind that of the upstream packet. As we shall see, the effect is due to the nonlinear motion of the resonant electrons. While moving from the left, the latter are successively bunched by the wave field, momentarily trapped, and positioned in phase with the wave potential. At this point ($x \sim 400\ \lambda_d$ for $t = 600\ \omega_p^{-1}$, $x \sim 500\ \lambda_d$ for $t = 720\ \omega_p^{-1}$) their bunching is reactive, which modifies the local dispersion relation leading to an elongation of the wavelength as discernible in the two bottom traces [*Denavit and Sudan*, 1972]. Now, because the wavelength stretches, the bunched electrons, which move ballistically, find themselves again in phase with the electric field after a short distance. There begins the downstream packet.

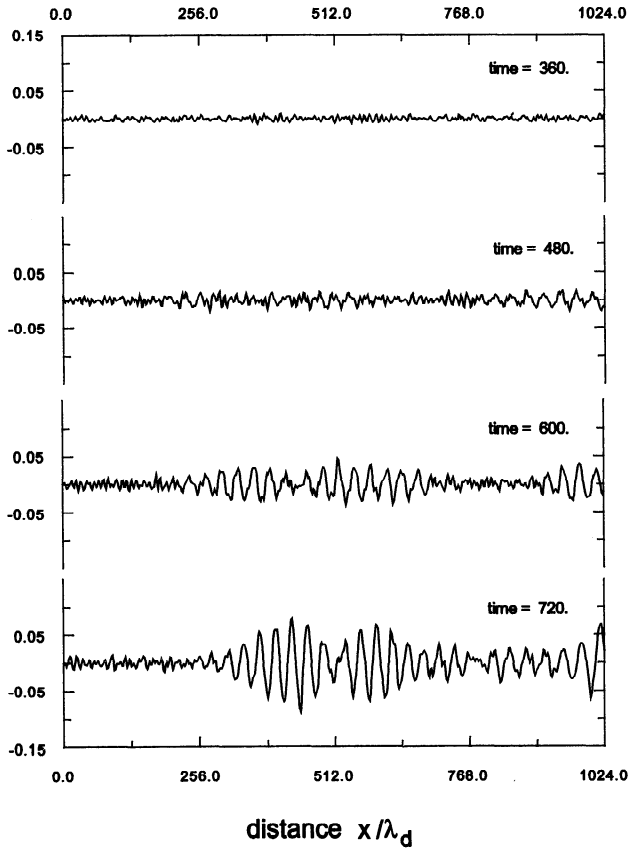

Figure 3. Four successive snapshots of the wave electric field showing two packets emerging out of the noise. E is in units of $(nT/\epsilon_0)^{1/2}$ and time in ω_p^{-1}.

3.1. Bunching in Phase Space

A snapshot of the perturbed distribution function associated with the bottom trace in Figure 3 is displayed in Figure 4. The portion of phase space covers several wavelengths from $x = 325\ \lambda_d$ to $x = 575\ \lambda_d$, while the range of velocities, $2 < v/v_e < 7$, extends from the core to the beam region. The quantity plotted, $(f(x,v) - F_e(v))/F_e$, is shown by means of contours, solid for an accumulation of electrons, dashed for a depletion thereof. To the left appears a series of bunches about $v \sim 3\ v_e$ which alternate sign following the wave electric field, shown in the rightmost panel. Between $4 < v/v_e < 6$ one can recognize, albeit in a somewhat roughened shape, the bunch-ellipses which were investigated in detail by the means of quiet simulations (MRE). As witnessed by the double chain of positive and negative bunches, the regime is nonlinear.

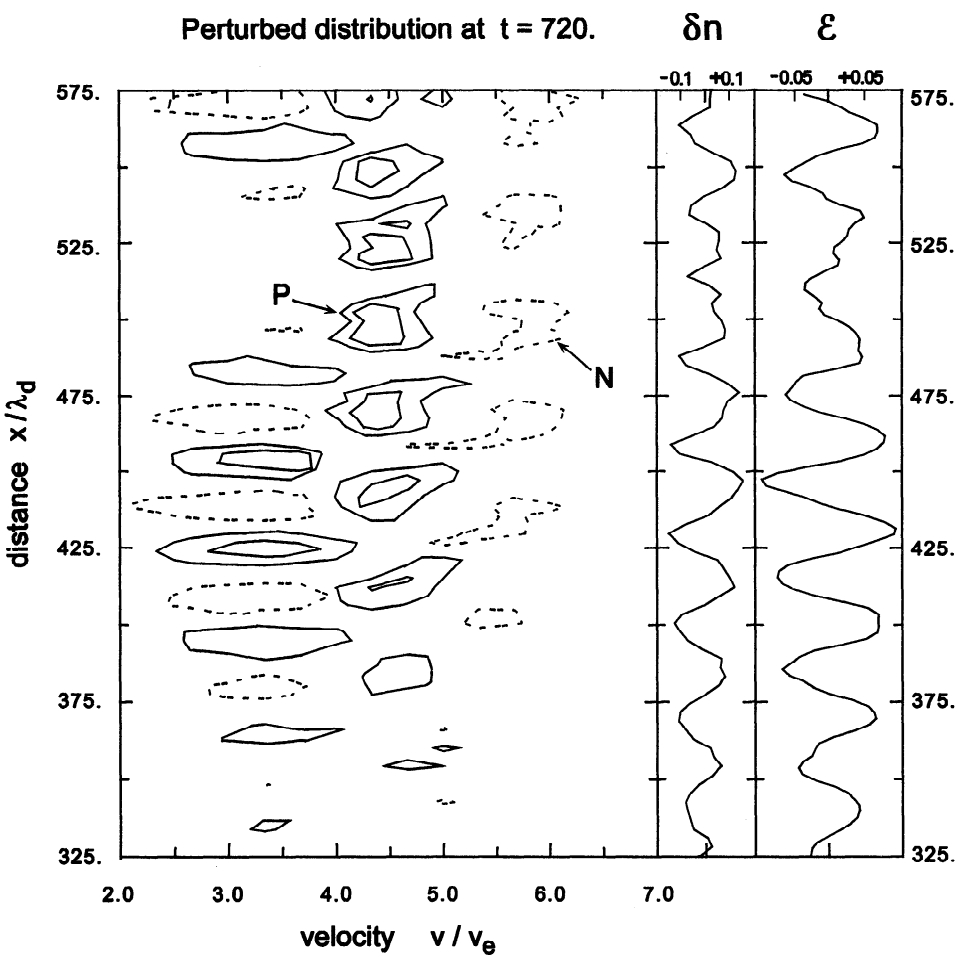

Figure 4. (Left) Snapshot of the perturbed distribution function associated with the wave field at $\omega_p t = 720$ shown in Figure 3 (bottom trace). Solid contours (+25%, +50%) indicate positive perturbations, dashed contour (-30%) negative perturbations. P and N denote positive and negative resonant bunches described in the test. (Middle) Resonant density perturbation. (Right) Instantaneous wave electric force acting upon the electrons, $\mathcal{E} \equiv -eE/(mv_e\omega_p)$.

It is worthwhile to examine the differences between what we call the nonresonant bunching, to the left ($v < 4v_e$), and the resonant bunching which occurs in the velocity interval $4 < v/v_e < 6$. First, the nonresonant bunching is reactive: the bunches of accumulated electrons are in phase with minima of the potential. Second, they follow the amplitude of the wave. So they maximize about $x/\lambda_d \sim 450$ and fall below contour level about $x/\lambda_d \sim 500$ to reappear about $x/\lambda_d \sim 550$ where the wave amplitude grows again. Third, the nonresonant bunching can be described by a linear solution to the Vlasov equation. Using equation (19b) of *Muschietti et al.* [1994], we rewrite the normalized perturbation as

$$\hat{f}_s \approx \frac{eE_a}{m\omega}\eta(x)\,\frac{F_e'}{F_e}\,\frac{v_p}{v - v_p}$$

where $\eta(x)$ describes the shape of the packet envelope with amplitude E_a and $\hat{f}_s = (f(x,v) - F_e(v))/F_e$ without the phase component. Considered as a function of v, and evaluated for $F_e(v)$ in Figure 2 the expression first grows monotonically from $v = 0$ because $v - v_p$ decreases (here $v_p = 5\ v_e$); the expression peaks at $v = 3.2\ v_e$ and then falls off about $4\ v_e$ due to the vanishing derivative F_e'. This is consistent with the contours obtained from the PIC simulation run. In addition, from the peak value $f_s \gtrsim 0.5$ reached, for example, at $v = 3.2\ v_e$, $x = 425\ \lambda_d$, one can deduct the electric field amplitude. One finds $eE_a/(mv_e\omega_p) \gtrsim 0.06$ in good agreement with the value reached by the function $\mathcal{E} \equiv -eE(x,t)/(mv_e\omega_p)$ plotted in the rightmost panel.

In contrast, the resonant bunching is nonlinear. The N (negative) bunches, associated with accelerated electrons, catch up with the P (positive) bunches, made of decelerated electrons. The behavior of the perturbed density in the resonant region, hence the current, is visible in the panel marked δn. Specifically, we plot the integral of the perturbed distribution between $4 < v/v_e < 7$ divided by $3v_eF_e(v_p)$; in other words, δn is normalized to the number density of resonant electrons, that is a number considerably smaller than the total number of electrons. As visible δn oscillates and peaks where the decelerating electric force of the wave on the electrons is the strongest, namely, $\mathcal{E}(x,t)$ is large

and negative. The resonant density δn is thus resistive within the packet and it reaches about 13%. We can use this information to evaluate the work done by the wave electric field and compare the result with the growth of the wave between the last two snapshots in Figure 3 ($600 < \omega_p t < 720$). We find $\langle \delta j \cdot E \rangle = 6 \times 10^{-5} nT\omega_p$ and $\langle E^2 \rangle = 4 \times 10^{-3} nT/\epsilon_0$, where the brackets mean the rms value over several periods. Therefore the growth rate is estimated to be $8 \times 10^{-3}\omega_p$, which means an amplification of the first packet by a factor 2.5 between $\omega_p t = 600$ and 720, in good agreement with what is observed.

3.2. Size of a Coherent Packet

After a few wavelengths, however, where the N bunches catch up with the P bunches, the oscillation in δn becomes uncertain. Plotting δn versus the potential shows them to be in phase, the electrons being bunched where the potential is positive and maximum. Following the simplified analysis in MRE we write the perturbed density as

$$\delta n = a_+ \cos(kx) \cos\left(\frac{\delta v}{v_p} kx\right) + a_- \sin(kx) \sin\left(\frac{\delta v}{v_p} kx\right) + a_- \quad (1)$$

where $a_\pm = a_P \pm a_N$ are the sum and difference of "weights" of the P and N bunches, respectively. The quantity δv represents the nonlinear orbit correction of the bunches and approximately equals $(|\mathcal{E}| v_e v_p)^{1/2}$. After a distance $\Delta x/\lambda = 0.25\, v_p/\delta v$ the first term in (1) vanishes while the second term, which has been steadily growing, becomes maximum. In Figure 4 this occurs about $x/\lambda_d \sim 500$. We can evaluate the change in the dispersion relation associated with that new reactive component. From (5a) of *Muschietti et al.* [1994] one has

$$k\lambda_d \left(1 - \frac{\omega_p^2}{k} \int dv \frac{F_e'}{kv - \omega}\right) = \frac{n_s}{\mathcal{E}} \quad (2)$$

where n_s is the new reactive component in units of the background density. The wavenumber change δk caused by the finite n_s is thus

$$\frac{\delta k}{k} = -\frac{1}{6}(k\lambda_d)^{-3} \frac{n_s}{\mathcal{E}}. \quad (3)$$

Using values from the simulation run, $n_s = 2 \times 10^{-4}$ and $\mathcal{E} = 0.02$, we obtain a local 20% decrease in the wavenumber. Therefore after one stretched wavelength the P bunches are again in phase with the electric field and drive up the second wave packet. In Figure 4 this occurs about $x/\lambda_d \sim 550$. Since the bunching is again resistive, n_s is negligible and the wavenumber returns to its original value.

That explains the phase shift between individual packets we observe in our simulations. Each packet has a maximum size corresponding to the spatial range over which the motion of the P and N bunches produces a resistive density perturbation. Because δv is finite, the ranges are bounded and separated by transitions where the bunching is locally reactive, distorting the phase relation between adjacent packets. The typical size for one packet is given, from (1), by

$$\mathcal{L} \sim \left(\frac{m\omega_p^2}{eE_a k}\right)^{1/2} \frac{\lambda}{2} = \frac{\pi}{\omega_p} \left(\frac{m\omega_p}{eE_a}\right)^{1/2} v_p^{3/2} \quad (4)$$

in which E_a is the amplitude of the electric field. For the snapshot of Figure 3 at $\omega_p t = 720$ this yields $\mathcal{L} \sim 4\lambda$, or 120 λ_d, in agreement with the two observed packets. The rightmost expression in (4) is handy for practical evaluations for it involves accessible quantities like the plasma frequency, the field amplitude, and the phase velocity, which one can estimate from the energetic electrons associated with the waves.

4. Saturation and Wave Transport

Long simulation runs were performed with and without ions so as to identify the saturation process. Some were carried out for up to as many as 21,000 time steps, or $t = 4200\ \omega_p^{-1}$. This amounts to about 18 ion plasma periods for a mass ratio of 1600. As time elapses, wave packets move on, leaving room for new packets to form. Figure 5 shows the results from such a run. Several

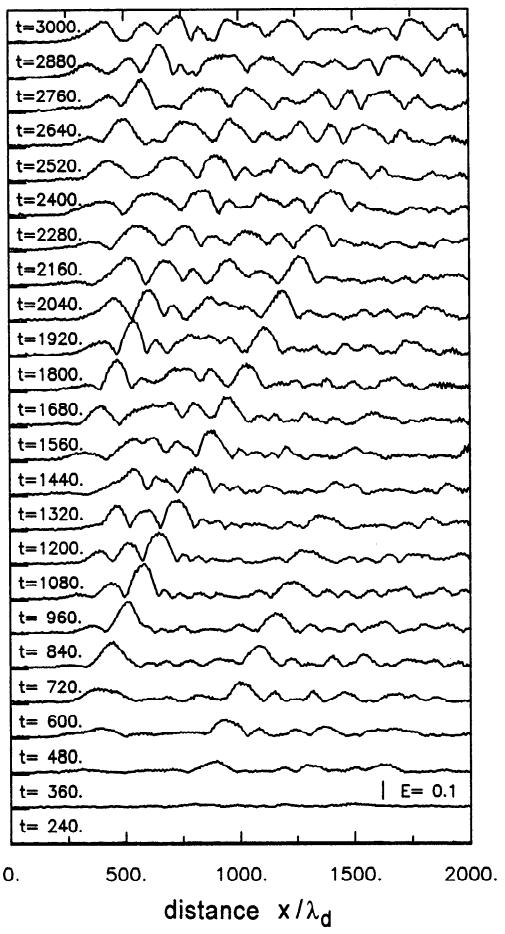

Figure 5. Profiles of the rms electric field recorded during a long simulation run. The scale is linear and the successive profiles are shifted vertically for presentation. E is in units of $(nT/\epsilon_0)^{1/2}$ and time t in ω_p^{-1}. The wave packets emerge out of the noise and progress downstream at the group velocity. More detailed profiles are visible in Figure 6.

profiles of the rms electric field are displayed as a function of distance. The successive times, which are in fact averaged over three plasma periods, are plotted with a vertical offset for presentation. One sees clearly the appearance of packets out of the noise, their motion toward increasing x, and the region progressively filling up with them. The wave intensity has definitely saturated. The rms electric field is of order 0.1 in normalized units, $E_{\rm rms} = 0.1\ (nT/\epsilon_0)^{1/2}$. The vertical scale used in Figure 5, which is indicated by a small bar in the lower-right corner, tends to compress the profiles. More details are visible in Figure 6 which uses a logarithmic display. Note the deep modulations in the field envelopes. In spite of the substantial level of wave energy, we find that the ions play a relatively little role in that regime. The saturation is attributed to wave transport. To check that such is the case, one needs to compute the free energy released from the beam electrons and check energy conservation. In a statistical equilibrium the wave energy carried away must balance the flux of free energy brought in.

4.1. Free Energy Released

The free energy that is constantly injected from upstream by the arrival of fresh beam electrons can easily be evaluated. At the left boundary the distribution function for positive v has the form shown in Figure 2 while at the right boundary it has plateaued. The energy difference is about $K = 1.2 \times 10^{-3} nT$. The group velocity v_g, on the other hand, equals 0.6 v_e as visible from Figure 5. Using

$$\frac{v_g}{2000} \int_0^{2000} \mathcal{W}\, dx = v_p\, K, \tag{5}$$

we obtain $\mathcal{W} \approx 10^{-2}$ in average over the interval. This agrees well with the simulation result and we conclude that the saturation of the instability is indeed due to wave transport.

A few words are in order regarding the group velocity. It was prematurely stated by MRE that the wave packet does not move in the nonlinear regime. This is not the case. In our system of beam, halo, and core, the presence of fast electrons increases the k dependence of the frequency above the Bohm-Gross value. On the other hand, the finite spatial grid of size Δ reduces the frequency by $k^2\Delta^2\omega_p/4$ [*Birdsall and Langdon*, 1985, p. 155]. The two effects offset each other, leaving the group velocity close to its classic value.

Another series of simulations was performed with model II of distribution function (see Table 1). Due to the enhanced halo, the beam component emerges less, whereby both the free energy and the linear growth rate are reduced. The weaker growth rate, $\gamma/\omega_p = 6 \times 10^{-3}$ instead of 1.2×10^{-2}, leads naturally to a longer growth length at the left end of the simulation box. The field emerges from the noise after $500\lambda_d$ instead of $250\lambda_d$. Besides that difference, wave packets are produced in a similar way. The study of their rms profiles, like the ones displayed in Figure 5, shows the following. First, the value of the electric field is diminished by a factor of 2 approximately. Second, though the packets are more irregular in shape, they are discernibly more stretched with somewhat larger gaps between them. The reduced electric field can easily be explained in terms of (5), considering that the free energy K available from distribution II is 4 times less than from distribution I.

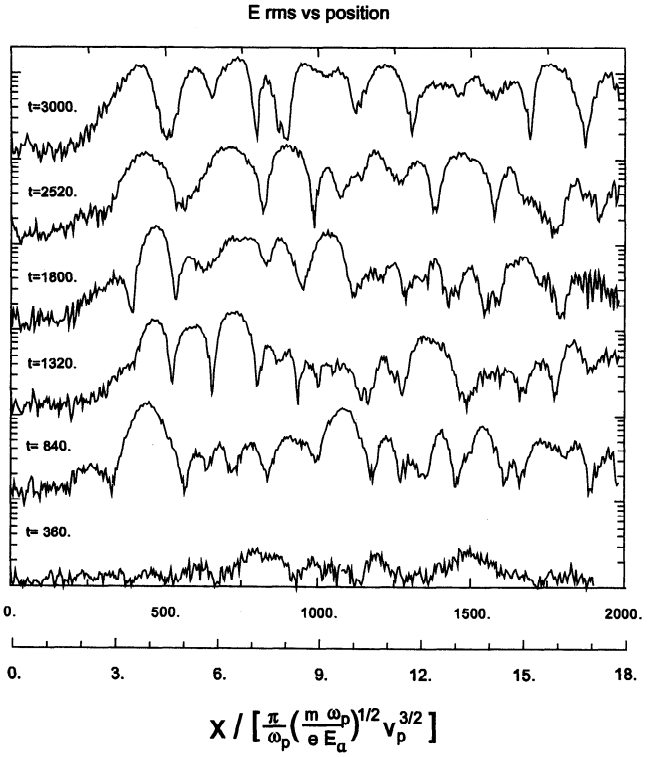

Figure 6. Six profiles of the rms electric field displayed with a logarithmic vertical scale. Time t in ω_p^{-1} unit. Note the deep modulations similar to the Ulysses data shown in Figure 1. The second horizontal axis at the bottom shows the spatial scaling based on (4) (see text for details).

4.2. Role of Ions

Figure 7 presents two examples of wave packets. These are snapshots of the electric field taken at late times well into the saturated regime. Though they are quite varied in size, the packets are generally short, just a few wavelengths long. Qualitatively there seems to be hardly a difference between the two panels, though one comes from a run including the ions, the other not. Figure 7b is a snapshot taken from a very long run ($\omega_p t = 4320$, or 21,600 steps) using particle ions with $T_i = T_e$. The wave energy density reaches $\mathcal{W} \approx 0.02$ in the intense second packet about $x \sim 700\lambda_d$, yet is generally of order 0.01. A wave spectrum analysis reveals indeed the nonlinear growth of backscatter Langmuir waves at smaller wavenumbers. Their intensity is, however, 2 orders of magnitude lower as compared to the primary spectrum.

Since a significant body of the foreshock literature invokes the electrostatic decay as a key feature [*Newman*, 1985; *Cairns and Robinson*, 1992b; *Thiessen and Kellogg*, 1993; *Robinson and Cairns*, 1995], we carried out a number of runs varying parameters. These results will be presented elsewhere, detailing nonlinear scattering

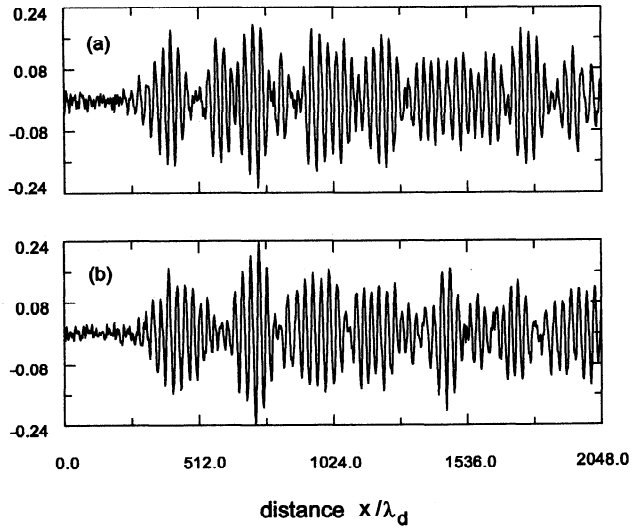

Figure 7. Snapshots of the wave electric field at late times: (a) with and (b) without ion dynamics. E is in units of $(nT/\epsilon_0)^{1/2}$.

off ion clouds and scattering off ion acoustic waves for various electron-to-ion temperature ratios (L. Muschietti et al., manuscript in preparation, 1996). Suffice it to say here that the growth of the secondary Langmuir waves observed in the simulations is of order

$$\gamma_{NL}/\omega_p \approx 10^{-1}\mathcal{W}.$$

Such an estimate is in line with results obtained for the nonlinear scattering off ion clouds [*Nicholson*, 1983; *Muschietti and Dum*, 1991]. Backscatter Langmuir waves being subject to Landau damping from the halo $\gamma_{L'}$, a large enough value of $\mathcal{W}$ is required to satisfy $\gamma_{NL} \gg \gamma_{L'} \sim 10^{-3}\omega_p$ and allow the secondary wave to grow to any significant extent. For the parameters of our simulations such is not the case.

The inhibition of the backscatter due to the halo was already recognized by *Newman* [1985]. This difficulty is overcome in recent Vlasov simulations of the electron foreshock by adding ion-acoustic fluctuations externally [*Goldman et al.*, 1995].

5. Discussion and Conclusion

In order to compare our simulation results to the observations, we make explicitly the following assumption. Equation (4) can be used to rescale our PIC results to the (small) fields observed in the foreshocks. An example of Langmuir envelope from Ulysses is shown in Figure 1. These are waves measured in the Jovian foreshock where the conditions were the following: plasma frequency $\omega_p \sim 3 \times 10^4$ rad/s, isothermal plasma with $T_e \sim T_i \sim 9$ eV, and a solar wind velocity of $V_{SW} \sim 400$ km/s. The waves were observed in association with a burst of suprathermal electrons in the 27—862 eV range [*Thiessen and Kellogg*, 1993].

Now, applying (4) for a field of 1 mV/m as observed and resonant electrons of 150 eV, which gives a phase velocity v_p of 7000 km/s, one obtains for characteristic scale $\mathcal{L}$ ~25 km. Figure 6 shows a sample of six wave envelopes extracted from the simulations reported in Figure 5. The vertical scale is logarithmic and the profiles have been shifted for presentation. Note the deep modulations in the envelopes. At the bottom, a second horizontal axis shows the assumed spatial scaling. Assuming further that the structure passes by the spacecraft because of the group velocity mainly (700 km/s for $v_p/v_e \sim 5$), we find that the distance 18 $\mathcal{L}$ is equivalent to 600 ms of the spacecraft time series that is displayed in Figure 1. The scale is of the right order and the comparison between the two figures is suggestive.

One can apply the same analysis to the waves measured upstream of the Earth's bow shock by *Etcheto and Faucheux* [1984]. The emissions close to the plasma frequency ($\omega_p \sim 1.8 \times 10^5$ rad/s) are made of a rapid succession of bursts lasting 30 to 40 ms (see their Figure 5). They are observed in regions of probable positive slope in the reduced distribution function above 300 eV, and reach a few millivolts per meter maximum at the edge of the foreshock. Applying again (4) with v_p ~12,000 km/s (400 eV) and $E_a = 1$ mV/m, one obtains $\mathcal{L}$ ~23 km, which should appear as a short 40-ms burst in the spacecraft frame.

In summary, we have studied the kinetic interaction taking place between energetic electrons and Langmuir waves. We used PIC simulations with open boundaries to account for the fast electrons constantly streaming into the wave region from outside. The resonant electrons are bunched in phase space forming bunch-ellipses. In the nonlinear regime the bunch-ellipses develop into a double chain. This changes the phase relation between oscillating current and wave field, causing the waves to grow in packets. The characteristic scale depends on the phase velocity (hence the beam velocity) and has a weak dependence on the amplitude of the electric field. We have applied the scaling to ISEE and Ulysses data. The comparison suggests that some of the observed modulations in the Langmuir envelope might in fact be due to nonlinearities in the resonant electrons. This explains why the modulations are seen with weak electric fields.

Acknowledgments. Several conversations with D. L. Newman regarding the foreshock are gratefully acknowledged by L.M. The computations were performed on the Cray C90 of the San Diego Supercomputer Center. The work was supported by NASA grant NAG5-2815, NAGW-3978, and NAS5-31283.

The Editor thanks K. B. Quest and another referee for their assistance in evaluating this paper.

References

Birdsall, C. K., and A. B. Langdon, *Plasma Physics via Computer Simulation*, p. 181, McGraw-Hill, New York, 1985.

Cairns, I., and P. A. Robinson, Strong Langmuir turbulence at Jupiter?, *Geophys. Res. Lett., 19*, 1069, 1992a.

Cairns, I., and P. A. Robinson, Theory for low-frequency modulated Langmuir wave packets, *Geophys. Res. Lett., 19*, 2187, 1992b.

Denavit, J., and R. N. Sudan, Effect of trapped particles on the nonlinear evolution of a wave packet, *Phys. Rev. Lett., 28*, 404, 1972.

Dum, C. T., Simulation studies of plasma waves in the electron foreshock: The generation of Langmuir waves by a gentle bump-on-tail electron distribution, *J. Geophys. Res., 95*, 8095, 1990a.

Dum, C. T., Simulation studies of plasma waves in the electron foreshock: The transition from reactive to kinetic instability, *J. Geophys. Res., 95*, 8111, 1990b.

Etcheto, J., and M. Faucheux, Detailed study of electron plasma waves upstream of the Earth's bow shock, *J. Geophys. Res., 89*, 6631, 1984.

Filbert, P. C., and P. J. Kellogg, Electrostatic noise at the plasma frequency beyond the Earth's bow shock, *J. Geophys. Res., 84*, 1369, 1979.

Fitzenreiter, R. J., A. J. Klimas, and J. D. Scudder, Detection of bump-on-tail reduced electron velocity distribution at the electron foreshock boundary, *Geophys. Res. Lett., 11*, 496, 1984.

Fitzenreiter, R. J., J. D. Scudder, and A. J. Klimas, Three-dimensional analytical model for the spatial variation of the foreshock electron distribution function: Systematics and comparisons with ISEE observations, *J. Geophys. Res., 95*, 4155, 1990.

Fitzenreiter, R. J., A. J. Klimas, A. F. Vinas, and K. W. Ogilvie, Electron foreshock observations by the WIND spacecraft (abstract), *Eos Trans. AGU, 76, (46)*, Fall Meet. Suppl., 473, 1995.

Goldman, M. V., D. L. Newman, J. G. Wang, and L. Muschietti, Langmuir turbulence in space plasmas, *Phys. Scr., in press*, 1995.

Hospodarsky, G. B., D. A. Gurnett, W. S. Kurth, and S. J. Bolton, High resolution measurements of Langmuir waves upstream of the Earth's bow shock, *Eos Trans. AGU, 72, (44)*, Fall Meet. Suppl., 390, 1991.

Hospodarsky, G. B., D. A. Gurnett, W. S. Kurth, M. G. Kivelson, R. J. Strangeway, and S. J. Bolton, Fine structure of Langmuir waves observed upstream of the bow shock at Venus, *J. Geophys. Res., 99*, 13,363, 1994.

Klimas, A. J., and R. J. Fitzenreiter, On the persistence of unstable bump-on-tail electron velocity distributions in the Earth's foreshock, *J. Geophys. Res., 93*, 9628, 1988.

Lacombe, C., A. Mangeney, C. C. Harvey, and J. D. Scudder, Electron plasma wave upstream of Earth's bow shock, *J. Geophys. Res., 90*, 73, 1985.

Muschietti, L., and C. T. Dum, Nonlinear wave scattering and electron beam relaxation, *Phys. Fluids B, 3*, 1968, 1991.

Muschietti, L., I. Roth, and R. E. Ergun, Interaction of Langmuir wave packets with streaming electrons: Phase-correlation aspects, *Phys. Plasmas, 1*, 1008, 1994.

Muschietti, L., I. Roth, and R. E. Ergun, Kinetic localization of beam-driven Langmuir waves, *J. Geophys. Res., 100*, 17,481, 1995.

Newman, D. L., Emission of electromagnetic radiation from beam-driven plasmas, Ph.D thesis, Univ. of Colo., Boulder, 1985.

Nicholson, D. R., *Introduction to Plasma Theory*, John Wiley, New York, 1983.

Robinson, P. A., and I. Cairns, Maximum Langmuir fields in planetary foreshocks determined from the electrostatic decay threshold, *Geophys. Res. Lett., 22*, 2657, 1995.

Robinson, P. A., and D. L. Newman, Strong plasma turbulence in the Earth's electron foreshock, *J. Geophys. Res., 96*, 17,733, 1991.

Scarf, F. L., D. A. Gurnett, W. S. Kurth, and P. L. Poynter, Voyager plasma wave measurements at Saturn, *J. Geophys. Res., 88*, 8971, 1983.

Skalsky, A., R. Grard, P. Kiraly, S. Klimov, V. Kopanyi, K. Schwingenschuh, and J. G. Trotignon, Simultaneous plasma wave and electron flux observations upstream of the Martian bow shock, *Planet. Space Sci., 41*, 183, 1993.

Thiessen, J. P., and P. J. Kellogg, Langmuir wave decay and collapse in the Jovian foreshock, *Planet. Space Sci., 41*, 823, 1993.

R.E. Ergun, L. Muschietti, and I. Roth, Space Sciences Laboratory, University of California, Berkeley, CA 94720-7450. (laurent@sunspot.ssl.berkeley.edu)

(Received January 2, 1996; revised March 18, 1996; accepted March 21, 1996.)